**Proceedings of the ASME 2022**
**International Design Engineering Technical Conferences and**
**Computers and Information in Engineering Conference**
**IDETC/CIE2022**
**August 14-17, 2022, St. Louis, Missouri**

**DETC2022-90500**

# DESIGN AND IMPLEMENTATION OF A POWER-DENSE, MODULAR, AND COMPACT SERPENTINE ARTICULATED TAIL

**Isaac Pressgrove, Yujiong Liu, Pinhas Ben-Tzvi***
Robotics and Mechatronics Laboratory
Mechanical Engineering Department
Virginia Tech
Blacksburg, VA, USA

## ABSTRACT

*Inspired by the many examples in nature, serpentine robotic tails can provide a means of expanding the feasible motion and general dexterity of mobile robots. Previous research has proven the effectiveness of robotic tails for the purpose of inertial reorientation through simulation of both simple pendulum and complex serpentine tails. There have been various experiments involving the integration of pendulum tails with a mobile base conducted to date. However, until now integration of more complex tail models has proven difficult. This paper presents an updated design of the existing Roll-Roll-Revolute Tail (R3RT) which can be readily integrated with a mobile base. The new design improves on the power density as well as form factor of the original design. Therefore, a design that is both more effective and easier to integrate with a mobile robotic base is synthesized. Kinematic and dynamic analysis are conducted to generate design targets. These targets are then met through the development of a power-dense actuator and evolution of a modular tail layout. CAD models of the new tail design integrated with the reduced complexity quadruped base are also reviewed. Finally, results of initial testing to prove the performance of the actuators are presented.*

Keywords: Robotic Tail, Robot Design, Design Integration

## 1. INTRODUCTION

In nature many animals have tails which are used alongside or in place of other limbs in order to manipulate, propel, maneuver, and/or stabilize [1]. Examples of this include: monkeys using their tails to grasp branches or to balance while walking [2, 3]; kangaroos using their tails as a fifth leg to support and contribute to their unique pentapedal gait [4]; common house cats compensating for disturbances while walking along beams [5]; and cheetahs using their tails to aid in highspeed turning, acceleration, and deceleration [6]. Seeing the many varied applications of tails in nature have led to researchers taking great interest in applying them towards increasing the range of feasible movements and overall agility of mobile robots.

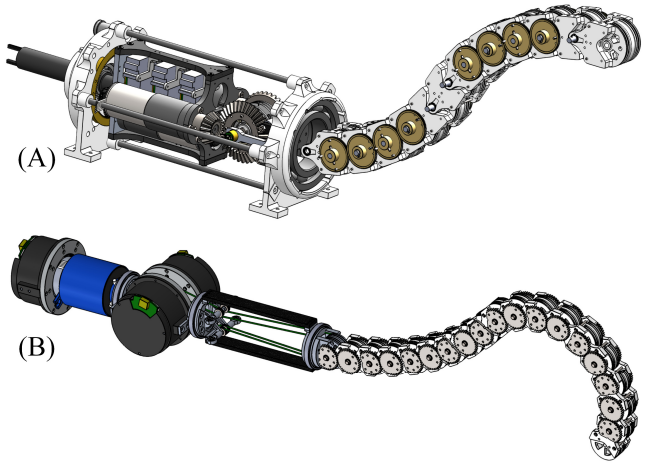


**FIGURE 1:** (A) THE ORIGINAL R3RT, (B) THE UPDATED R3RT-V2 DESIGN

According to a state of the art review conducted by Saab et al. [7] the earliest example of a robotic tail used for inertial reorientation was the Uniroo robot, a single legged hopping robot which used a tail to control pitch [8]. Following Uniroo there was Zappa [9], a quasi-passive bipedal robot. Zappa used a single degree of freedom (DOF) pendulum tail to induce movement of the legs resulting in locomotion. After Zappa there

*Corresponding author – bentzvi@vt.edu

was a significant uptick in robotic tail research. RJ Full et al. modelled a gecko's use of its tail for mid-air reorientation as a two DOF pendulum attached to the body via a universal joint. The model was then verified by adding a single DOF tail to a quadruped, Stickybot, capable of midair righting along the robot's longitudinal axis [10]. Continuing research based on the findings from the analysis of gecko tails Full et al. also tested planar pendulum tails for mid-air inertial reorientation on two other robots. These two are, a four wheeled robot Tailbot [11] and the six legged robot X-RHex Lite [12]. Another example of using a tail for mid-air pitch control include Xiao et al. miniature jumping robot [13]. Research has also been conducted on applications for added stability and control during locomotion. The kangaroo robot designed by Lin et al. utilized a tail to control pitch of the robots body during locomotion [14, 15]. The TAYLRoACH implemented a vertically pinned tail to add yaw position control while running [16]. In a similar vein, Braae et al. added a planar tail in two different configurations to a wheeled robot to aid in dynamic handling similar to how a cheetah uses its tail while running. The first configuration had the tail pinned to rotate about the vehicles longitudinal axis to improve highspeed cornering [17]. The second rotated the pin 90 degrees so that the tail would aid in pitch control during acceleration and deceleration [18]. A final and unique implementation of pendulum tails for inertial reorientation is the climbing robot ROCR developed by Fehlberg et al. which used a tail to induce both quasi-static and dynamic climbing motions [19].

More recent research has begun to explore designs of serpentine robotic tails. Serpentine tails show promise in replicating and in some instances improving upon the inertial reorientation capabilities of pendulum tails [20, 21]. As well, serpentine tails open up new possibilities for tail use. Examples include using tails for self-righting, gait augmentation, and adding manipulators. Some of the latest designs include the Discrete Modular Serpentine Tail (DMST) [22, 23], Universal-Spatial Robotic Tail (USRT) [24-26], RML Tail [27], and the Roll-Roll-Revolute Tail (R3RT) [28, 29]. Though prototypes exist for all of these tails and simulations have been conducted to show their ability as inertial reorientation devices for quadrupedal and/or bipedal bases, none have yet been integrated with a physical base. The authors posit that this is in large part due to size and inconvenient shape of the cable actuation units associated with them.

Therefore, this paper aims to update the R3RT to improve power density and increase ease of integration with an untethered mobile base. To do this, the tail actuation architecture will need to be capable of producing cable tensions sufficient to achieve the previously seen tail's performance while being significantly more compact and modular than existing designs.

The following sections are organized as follows. Section 2 presents the dynamic model used to set design targets. Section 3 describes the mechanical design of the architecture. Section 4 covers the prototyping and preliminary experimental results. The conclusion recaps the main points of this paper and discusses future work.

## 2. DYNAMICS AND DESIGN TARGETS

This section presents the changes to the kinematics of the R3RT tail structure from those used in previous papers. Then the simulation which was used to define the actuation requirements will be described. Finally, the results of simulation will be presented and translated into design requirements.

The kinematics, dynamics, and associated simulation environment used in this paper are based off of those presented in [30]. This paper presents two updates to the kinematic formulation to allow for greater flexibility in investigating design parameters. Those changes are to make the number of links in the tail and location of the center of mass (COM) of the base link variable. Though neither of these changes fundamentally change the kinematics or dynamic modeling of the tail, they do impact overall performance.

The tail, previously composed of 12 links, is now composed of N links split into two planar bending segments composed of $N/2$ links attached to a base link, which provides overall rolling motion. In this way the tail can be said to have 3 DOFs defined by the base link rolling angle $\alpha$ and the two planar bending angles for the links within each planar bending segment, $\beta_1$ and $\beta_2$. The body fixed frames $\sum J_i \coloneqq (J_i, \mathbf{x}_i, \mathbf{y}_i, \mathbf{z}_i)$, $\sum T \coloneqq (T, \mathbf{x}_0, \mathbf{y}_0, \mathbf{z}_0)$, and $\Sigma P \coloneqq (P, \mathbf{x}_p, \mathbf{y}_p, \mathbf{z}_p)$ for links $i$ through $N$, the base link, and reduced complexity quadruped (RCQ) base respectively are defined as shown in Fig. 2. It is important to note is that $\sum T$ is located such that $\mathbf{y}_0$ coincides with $\mathbf{y}_p$ and $\mathbf{x}_0$ coincides with the x-axis of joint 1. The global fixed reference frame is defined as $\Sigma S \coloneqq (S, \mathbf{x}_s, \mathbf{y}_s, \mathbf{z}_s)$. Further detail on modelling can be found in [21].

Important kinematic equations that differ from those described in [21] due to the aforementioned changes to link count and base link COM location are shown below. In these equations, a rotation matrix denoted by ${}^{B}\mathbf{R}_{A}$ is defined as the general rotation from frame $\Sigma A$ to $\Sigma B$. $\mathbf{R}_x$ and $\mathbf{R}_y$ are the principal rotation matrices with respect to x and y axis. Vectors $\mathbf{p}_{0,com}$ and $\mathbf{p}_t$ are defined as the position of the COM of the base link, $C_0$, and the location of the origin of the base link, $T$, in $\Sigma S$. ${}^{0}\mathbf{p}_{C0}$ is defined as the local vector from T to $C_0$ in $\Sigma T$.

$$ {}^{S}\mathbf{R}_i = \begin{cases} {}^{S}\mathbf{R}_P\mathbf{R}_y(\alpha), i = 0 \\ {}^{S}\mathbf{R}_P\mathbf{R}_y(\alpha)\mathbf{R}_x(i\beta_1), 1 \le i \le \frac{N}{2} \\ {}^{S}\mathbf{R}_P\mathbf{R}_y(\alpha)\mathbf{R}_x\left(6\beta_1 + (i - \frac{N}{2})\beta_2\right), \frac{N}{2} \le i \le N \end{cases} \quad (1) $$

$$ \mathbf{p}_{\mathbf{0},com} = \mathbf{p}_{\boldsymbol{t}} + {}^{S}\mathbf{R}_0\,{}^{0}\mathbf{p}_{C0} \quad (2) $$

The necessary Jacobians can be obtained by differentiating Eqs. (1) – (2) and factoring out the generalized coordinates. The corresponding Jacobians are listed in Eqs. (3) – (5) where $\mathbf{u}_{m,n}$ is the $m$ dimension unit column vector with 1 on the $n$-th entry. The tilde over a vector indicates its skew symmetric expansion.

$$\mathbf{J}_{i,\omega} = \begin{cases} [\mathbf{0}_{3\times3} \quad \mathbf{I}_{3\times3} \quad \mathbf{0}_{3\times3}] + \mathbf{y}_0\mathbf{u}_{9,7}^T, i = 0 \\ \mathbf{J}_{i-1,\omega} + \mathbf{x}_0\mathbf{u}_{9,8}^T, \quad 1 \le i \le \dfrac{N}{2} \\ \mathbf{J}_{i-1,\omega} + \mathbf{x}_0\mathbf{u}_{9,9}^T, \quad \dfrac{N}{2} \le i \le N \end{cases} \tag{3}$$

$$\mathbf{J}_{C0} = -(\widetilde{{}^S\mathbf{R}_0\,{}^0\mathbf{p}_{C0}})\mathbf{J}_{0,\omega} \tag{4}$$

$$\mathbf{J}_{0,com} = \mathbf{J}_t + \mathbf{J}_{C0} \tag{5}$$

Since the changes to the above equations do not directly appear in the equations of motion, the construction of the dynamics is not changed. Details on the dynamic modeling of R3RT system can be found in [30].

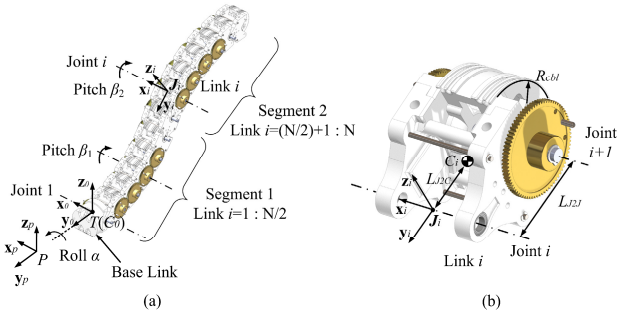


**FIGURE 2:** (A) KINEMATIC CONFIGURATION OF THE R3RT. (B) KINEMATIC CONFIGURATION FOR THE $i$-TH LINK

The RCQ was primarily designed to perform maneuvering task as defined and simulated in [30]. Therefore, the design requirements for the tail presented in this paper are generated using the existing maneuvering simulation with all of the same parameters as set forth in [30] except for the change in number of links and the addition of the new parameter ${}^0\mathbf{p}_{C0}$. When $N = 12$ and ${}^0\mathbf{p}_{C0} = \mathbf{0}$ the simulation is unchanged.

To set a baseline, the optimal tail length of two times the body length and a tail mass of 0.09 times the body mass was used with $N = 12$ and ${}^0\mathbf{p}_{C0} = \mathbf{0}$. The results of this combination showed a peak power of 135W was required, which is consistent with the results in [30]. To add more detail to this requirement, the speed and actuation effort of each DOF were also recorded. The roll actuator effort and velocity are measured in newton-meters and rad/s, respectively. Since the planar bending is driven by cables, the force and velocity for bending are measured in newtons and m/s, respectively. The results are shown in Fig. 3. Beyond the baseline, one additional trial was run with the COM of the base link moved to the center of the quadruped (${}^0\mathbf{p}_{C0} = [0 \;\; 0.15 \;\; 0]^T$) and $N = 18$. It was found that these two changes resulted in a much lower peak power requirement of 90 W and correspondingly lower actuator effort and velocity, as shown in Fig. 4.

Based on these findings, the design requirements were decided to be as follows: A minimum peak power output of 100 W for all actuators, A roll actuator capable of outputting 9 Nm, bending actuators capable of outputting 150 N, and the ability to have the center of mass of the actuation unit be located in the center of the body.

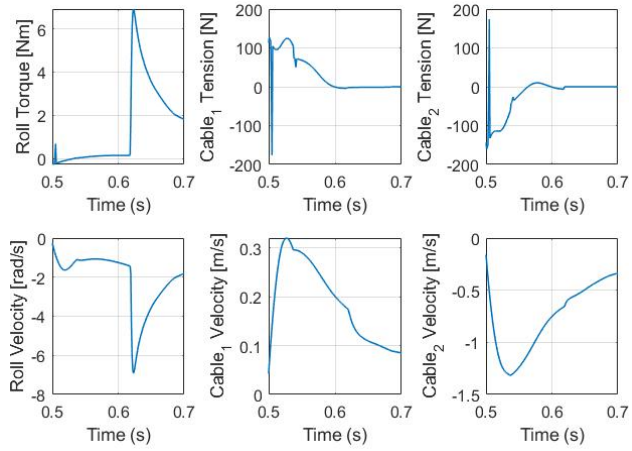


**FIGURE 3:** ACTUATION EFFORT AND VELOCITY FOR BASELINE VALUES

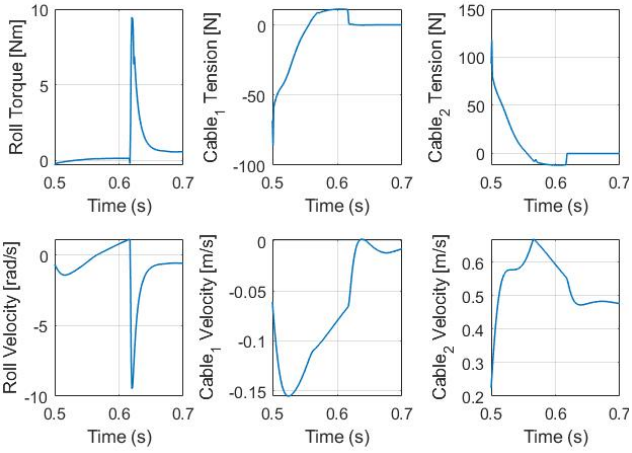


**FIGURE 4:** 18-LINK TAIL WITH REPOSITIONED BASE LINK COM

## 3. MECHANICAL DESIGN

This section details the mechanical design of the tail actuation architecture and how it meets the design requirements from the previous section while improving upon prior designs.

As noted previously, one of the largest obstacles to integrating an articulated tail with a mobile base is the mass of the actuation unit. In simulation the base link represents the actuation unit. Since the dynamic targets were set using the predicted 6 kg RCQ model from [30], this iteration aims for an actuation unit totaling a mass of no more than 1 kg.

Also identified as an obstacle to integrating existing articulated tail designs with a mobile base is the relatively large size and bulky fixed shape. This causes two main issues. First, it is difficult to package the actuation units in a compact chassis with other critical components. Second, it significantly limits

flexibility in locating the center of mass of the mobile base, which is heavily influenced by the mass of the tail actuation unit. To remedy these issues, the tail actuation architecture presented will be modular, thereby allowing for varying distances between the roll actuator, bending actuators, tensioner, and tail base.

### 3.1 Actuator Design

The first step to achieving the dynamic targets, total mass, and flexible packaging goals is to design a compact and power dense actuator. To do this, inspiration was taken from the actuator designed for the MIT Cheetah robot series. Their actuator features a brushless pancake style out runner motor attached to a planetary gearbox with an onboard motor controller board [31]. This style of actuator provides a lightweight compact package capable of a relatively high peak torque output. These attributes make the layout well suited for driving the quick but highly dynamic movements of a robotic tail.

In order to minimize packaging space requirements, the tail actuator must be as compact as possible. This is especially true for the planar bending actuators, which need to be able to rotate with the tail in order to avoid complicated cable routings. Because of this, the RCQ torso width of 200 mm minus an additional 50 mm to account for other components that may be needed was considered to be the limit of the packaging for the bending actuators. In order to meet the modular requirement, it was decided that the actuator developed should be able to drive any of the DOFs with little or no modifications. These, in combination with the power and peak torque requirements from the previous section, make up the complete set of requirements for the actuators.

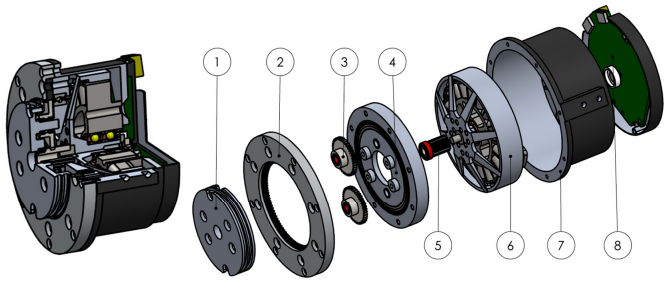


1 Actuator Output
2 Ring Gear
3 Planets
4 Planet Carrier
5 Sun
6 T-Motor MN6007
7 Back Housing
8 Controller

**FIGURE 5:** EXPLODED VIEW OF THE ACTUATOR

For motor selection, it was found that the T-Motor MN6007 proved to be an attractive option due to its reported peak power of 936 W, peak torque of 1.3 Nm, and relatively small outer diameter of 67 mm. To bring the torque output up to meet the design requirement of 9 Nm, the actuator would need a gear reduction of at least 7. Based on available gears, it was decided that a single stage planetary reduction of 7.25 would be used. To meet the linear force output requirement, the pulleys driving the planar bending would need to have a radius no larger than 63 mm.

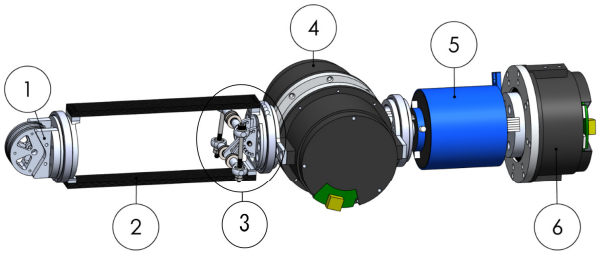


1 Base Link
2 Carbon Fiber Spine
3 Tensioner
4 Planar Bending Actuator Pair
5 120 Amp Slip Ring
6 Roll Actuator

**FIGURE 6:** TAIL ACTUATION ASSEMBLY

Fig. 5 shows an exploded view of the final actuator design. The actuator has an outer diameter of 82 mm and axial length of 53 mm. The actuator design includes a built-in pulley with a radius of 23.5 mm as part of the planet carrier which is included in the 53 mm axial length. This means that when paired together, as shown in Fig. 6, with 0.5 mm clearance between them, the total axial length is only 106.5 mm with a maximum edge to edge dimension of 125 mm across the diagonal.

The actuator has a mass of 460 g, which would violate the design requirement set for the mass of actuation unit if all three actuators rotated as they did in the previous R3RT design. However, because the roll actuator is now fixed to the chassis and does contribute to the rotating mass, it can be considered part of the body. More detail on the total mass of the actuation unit and layout will be given in section 3.3.

The final product of this design is a single 900 W actuator with a mass of only 460 g, which can be used for all three DOFs. The actuator provides a predicted peak torque of 9 Nm and peak pulling force of 380 N and has a power density of 1.95 W/g.

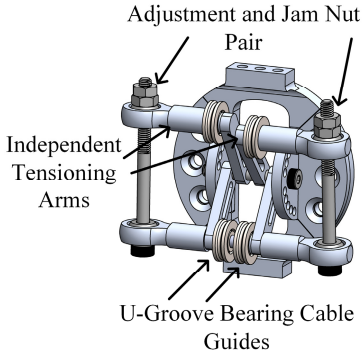


**FIGURE 7:** TENSIONER MECHANISM

### 3.2 Tensioner Design

A compact, reliable, and easily adjustable tensioner is crucial to the proper operation of the tail. In testing the original R3RT tail design, it was found that the lack of a reliable tensioner made control of the bending DOFs more difficult and in some extreme cases caused complete failure by allowing the cable to jump off the pulley.

For the tensioner to be considered reliable, it must resist loosening when repeatedly exposed to shock loading. To ensure that the tensioner for this tail design does not loosen, it is tightened by tightening an adjustment nut on a bolt, which is then secured with a jam nut. This way not only does the jam nut prevent the adjustment from backing off, but the force applied against the adjustment method is guaranteed not to be in a direction which could rotate the nut.

### 3.3 Actuation Unit Layout and Integration with Mobile Base

The actuators take care of the design requirements except for one. That is the need for the COM of the actuation unit to be located as close as possible to the center of the mobile base. As was shown in [32], the location of the system COM has a large impact on the ability of the robot to successfully complete a maneuvering task. It is therefore advantageous to be able to have flexibility in locating the actuation unit COM. For the RCQ layout, it was decided that keeping the actuation COM as close to the geometric center of the robot would be best, but in other applications it may be preferential to have the COM be located elsewhere. In order to provide this flexibility, the actuation unit presented here has a modular design split into three main components connected by a rigid spine. As shown in Fig. 6, these three components are the base link, planar bending actuator pair, and roll actuator. In this iteration, the tensioner is paired with the planar bending actuators, but it could just as easily be paired with the base link if this was preferred. The Roll actuator and planar bending pair are connected via a 12 mm rod which passes through the 120 A slip ring and transmits the rolling motion. The planar bending pair is then connected to the base link via a pair of carbon fiber plates, which are spaced apart to provide maximum torsional stiffness without compromising packaging space within the RCQ chassis.

The combination of the power dense actuators which provide nearly 2 W/g, compact and reliable tensioner mechanism, and unique modular layout make this actuation module easy to integrate with a mobile robotic base. To give context to the scale of improvement made by this design, it will be compared against the original R3RT. The original design used three Maxon EC-i40 motors. The total mass of actuation module is 6.4 kg giving it a combined power density of 0.047 kW/kg. The total mass of the new actuation unit is a full quarter of the previous at 1.6 kg giving it an overall peak power density of 1.7 kW/kg. The T-Motor does not provide a clear continuous power rating but taking the standard estimation of continuous power being one fourth of the peak, the new actuation module would have a power density of 0.425 kW/kg. This is a tenfold improvement over the existing R3RT design. Additionally, since the roll actuator is fixed to the chassis and non-rotating in this new design, it can be considered part of the chassis rather than actuator, as it is in the existing design. This helps to reduce rolling torque requirements and overall power draw of the system. This means that in simulation the actuation unit will only be considered to have a mass of 1.14 kg. Calculations for the moment of inertia will also exclude the roll actuator. As well as being only one fourth the mass and ten times more power dense than the original R3RT, the modular layout significantly improves ease of packaging and integration. This is poignantly displayed in Fig. 8 where the new design can be seen neatly packaged into the base to fit around other actuators and the battery pack with additional space for controller boards left open.

The increased power density, lower weight, and flexible layout will make integrating a tail and mobile base significantly easier in the future. This will facilitate the movement of future research into the performance and applications of articulated serpentine tails out of simulation and into real world testing.

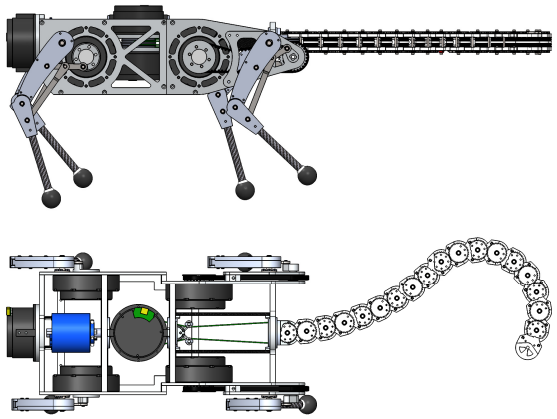

**FIGURE 8:** FINALIZED CAD MODEL OF R3RT-V2 INTEGRATED WITH RCQ BASE

## 4. PRELIMINARY EXPERIMENTS

To verify the performance of the new design before physical prototypes were manufactured, two additional simulations were conducted. The first simulation used the same parameters for the base and 18-link tail as before, but substituted in values for the mass, moment of inertia, and COM location of the new actuation unit as well as updated saturation limits based on the new actuators. This simulation showed a peak power requirement of 95.6 W, a peak rolling torque of 9 Nm, and a peak cable tension of 90 N. This confirmed that the previously set power and actuation effort targets were still valid. The slightly higher values from this simulation versus the original can likely be explained by the slight increase of mass in the effective base link from 1 kg to 1.14 kg. The second simulation brought the full model up to date with the finalized CAD for both the RCQ base and 18-link tail by updating all masses, moments of inertia, link lengths, and COM locations to match the CAD. This simulation again verified design targets as well as gave a more thorough comparison of how well the integrated design met design goals beyond just comparing values against the previously set targets. The values used for this final simulation are listed in Table 1 and plots of the actuator effort and velocity can be seen in Fig 9. With all values were updated to match the finalized CAD, the simulation predicted a peak power requirement of only 63.7 W, a peak rolling torque of 8 Nm, and a peak cable tension of 85 N. These

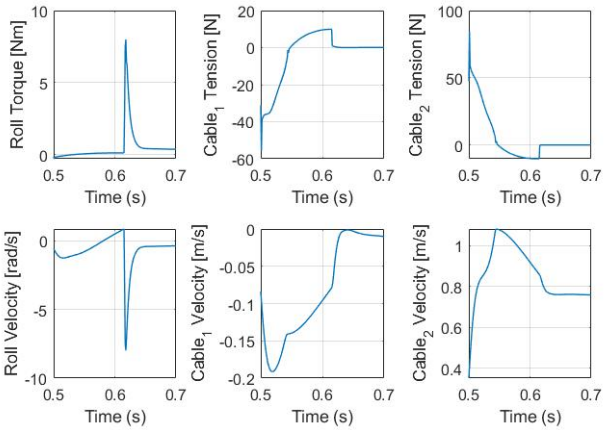


**FIGURE 9:** SIMULATION RESULTS WITH VALUES FROM FINALIZED CAD

results give a high degree of confidence that the targets set earlier will be sufficient.

Two initial experiments were conducted to test the performance of the actuators. The first experiment tested the peak torque output of the actuator and the second looked at the power efficiency. For both experiments, the actuator was powered by a 900 W power supply set to supply a constant 24 volts.

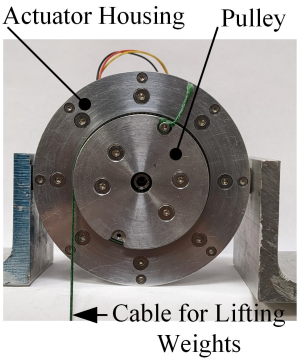


**FIGURE 10:** ACTUATOR PROTOTYPE

The first experiment was conducted by tying weights of increasing mass to the end of a cable wrapped around the actuator pulley (shown in Fig. 10) and commanding a 5 rad/s rotation. This experiment yielded several important conclusions. First, the actuator is capable of lifting 15 kg at a max angular speed of 4.23 rad/s, corresponding to an output of 147 N cable tension and 3.45 Nm of torque while only drawing 2.6 amps. Second, the PID controller currently programmed into the motor controller board has significant steady state error and was struggling to reach the commanded speed under any given load. Third, there is an issue with voltage spikes during initial startup of the actuator when attempting to lift higher loads leading to shorting out of the controller board protection circuit. The first piece of information is very promising since it shows that the actuator can nearly meet the cable tension requirement as is and is over a third of the way to the torque requirement while drawing less than a tenth of the motors rated peak current of 40 amps. Once the issues with the controller are resolved and the actuator is able to draw full current, there should be no issue meeting the full design requirements.

**TABLE 1**: CAD Model Properties Used in Simulation

| Property Name | Value |
|---|---|
| Base Link Mass [kg] | 1.14 |
| Base Link MOI [$\mathrm{kg \cdot m^2}$] | $\mathrm{diag}([5.57\ 1.05\ 5.18]) \times 10^{-3}$ |
| Tail Link Mass [kg] | 0.023 |
| Tail Link MOI [$\mathrm{kg \cdot m^2}$] | $\mathrm{diag}([4.98\ 3.69\ 6.14]) \times 10^{-6}$ |
| RCQ Base Mass [kg] | 5.93 |
| RCQ MOI [$\mathrm{kg \cdot m^2}$] | $\mathrm{diag}([8.23\ 6.49\ 13.08]) \times 10^{-2}$ |

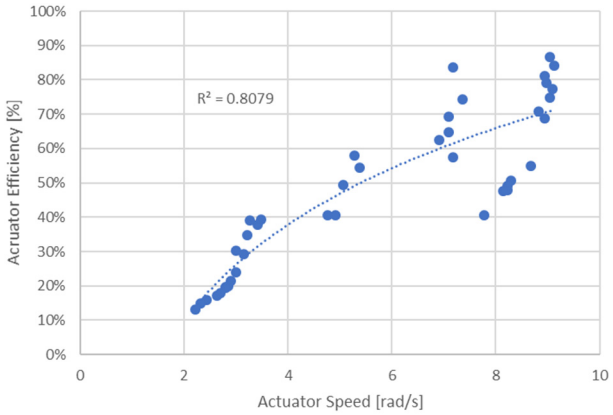


**FIGURE 11:** ACTUATOR EFFICIENCY VS SPEED

The second actuator test looked into the efficiency of the actuator under different loads at a range of speeds. For this experiment the actuator was made to lift a 5, 10, and 15 kg mass at commanded speeds of 5, 7, and 9 rad/s. The power in based on current draw at a fixed voltage was then compared against the power out calculated as $torque \times speed$. As can be seen in Fig. 11, the efficiency follows a roughly logarithmic trend increasing to be close to 70% efficient at higher speeds. This information is important to quantifying the performance of the gearbox in the actuator design. According to the MN6007 data sheet, the motor has an average efficiency of 78% at speeds from 289 rad/s to 547 rad/s. Based on this and the apparent flattening of the efficiency curve in the data show in Fig. 11 at around 9 rad/s actuator output speed (65 rad/s motor speed), a rough estimate for the actuator efficiency can be obtained. To do this, the average efficiency for speeds above 8 rad/s is obtained and divided by the average 78% efficiency of the MN6007. The average efficiency above 8 rad/s is 65%, which yields a gearbox efficiency of 83.8%. This is low for a single stage planetary gearbox, which would normally be expected to perform above 90% efficiency but given that the number of data points used is small and relatively spread out, and

the data is taken well below the efficient range for the motor, it can be considered a good initial result.

The simulation results found using the most accurate values currently available, combined with promising initial experiments with a prototype actuator, give a high level of confidence that the full prototype of the tail actuation module will perform all desired task without issues.

## 5 CONCLUSION AND FUTURE WORK

This paper presented an improved design of the R3RT, which now consists of more power dense actuators, exhibits modularity, and can be readily integrated into a mobile base. Based on simulation results and prior experience with articulated tail prototypes, some new design requirements were set forth. These requirements were then met through the development of a new power dense actuator, reliable and compact tensioner, and modular layout for the actuation unit. Simulations were rerun with values based on finalized CAD to compare to predicted design performance to the benchmarks. Initial testing was conducted with the first actuator prototype to confirm predicted performance. Future work will include full construction of the proposed design and integration with the RCQ base. This system will then be used to further investigations into articulated serpentine tails.

## ACKNOWLEDGMENTS

This material is based upon work supported by the National Science Foundation under Grant No. 1906727.

## REFERENCES

[1] G. C. HICKMAN, "The mammalian tail: a review of functions," *Mammal review,* vol. 9, no. 4, pp. 143-157, 1979.

[2] J. W. Young, G. A. Russo, C. D. Fellmann, M. A. Thatikunta, and B. A. Chadwell, "Tail function during arboreal quadrupedalism in squirrel monkeys (Saimiri boliviensis) and tamarins (Saguinus oedipus)," *Journal of Experimental Zoology Part A: Ecological Genetics and Physiology,* vol. 323, no. 8, pp. 556-566, 2015.

[3] M. Bezanson, "The Ontogeny of Prehensile-Tail Use in C ebus capucinus and A louatta palliata," *American journal of primatology,* vol. 74, no. 8, pp. 770-782, 2012.

[4] S. M. O'Connor, T. J. Dawson, R. Kram, and J. M. Donelan, "The kangaroo's tail propels and powers pentapedal locomotion," *Biology letters,* vol. 10, no. 7, p. 20140381, 2014.

[5] C. Walker, C. J. Vierck Jr, and L. A. Ritz, "Balance in the cat: role of the tail and effects of sacrocaudal transection," *Behavioural brain research,* vol. 91, no. 1-2, pp. 41-47, 1998.

[6] A. M. Wilson, J. Lowe, K. Roskilly, P. E. Hudson, K. Golabek, and J. McNutt, "Locomotion dynamics of hunting in wild cheetahs," *Nature,* vol. 498, no. 7453, pp. 185-189, 2013.

[7] W. Saab, W. S. Rone, and P. Ben-Tzvi, "Robotic tails: a state-of-the-art review," (in English), *Robotica,* Review vol. 36, no. 9, pp. 1263-1277, 2018.

[8] G. J. Zeglin, "Uniroo--a one legged dynamic hopping robot," Massachusetts Institute of Technology, 1991.

[9] F. J. Berenguer and F. M. Monasterio-Huelin, "Zappa, a quasi-passive biped walking robot with a tail: Modeling, behavior, and kinematic estimation using accelerometers," *IEEE Transactions on Industrial Electronics,* vol. 55, no. 9, pp. 3281-3289, 2008.

[10] A. Jusufi, D. T. Kawano, T. Libby, and R. J. Full, "Righting and turning in mid-air using appendage inertia: reptile tails, analytical models and bio-inspired robots," *Bioinspir. Biomim.,* vol. 5, no. 4, p. 045001, 2010.

[11] E. Chang-Siu, T. Libby, M. Tomizuka, and R. J. Full, "A lizard-inspired active tail enables rapid maneuvers and dynamic stabilization in a terrestrial robot," in *2011 IEEE/RSJ International Conference on Intelligent Robots and Systems*, 2011: IEEE, pp. 1887-1894.

[12] A. M. Johnson, T. Libby, E. Chang-Siu, M. Tomizuka, R. J. Full, and D. E. Koditschek, "Tail assisted dynamic self righting," in *Adaptive Mobile Robotics*: World Scientific, 2012, pp. 611-620.

[13] J. Zhao, T. Zhao, N. Xi, F. J. Cintrón, M. W. Mutka, and L. Xiao, "Controlling aerial maneuvering of a miniature jumping robot using its tail," in *2013 IEEE/RSJ International Conference on Intelligent Robots and Systems*, 2013: IEEE, pp. 3802-3807.

[14] G.-H. Liu, H.-Y. Lin, H.-Y. Lin, S.-T. Chen, and P.-C. Lin, "Design of a kangaroo robot with dynamic jogging locomotion," in *Proceedings of the 2013 IEEE/SICE International Symposium on System Integration*, 2013: IEEE, pp. 306-311.

[15] G.-H. Liu, H.-Y. Lin, H.-Y. Lin, S.-T. Chen, and P.-C. Lin, "A bio-inspired hopping kangaroo robot with an active tail," *Journal of Bionic Engineering,* vol. 11, no. 4, pp. 541-555, 2014.

[16] N. J. Kohut, A. O. Pullin, D. W. Haldane, D. Zarrouk, and R. S. Fearing, "Precise dynamic turning of a 10 cm legged robot on a low friction surface using a tail," in *2013 IEEE International Conference on Robotics and Automation*, 2013: IEEE, pp. 3299-3306.

[17] A. Patel and M. Braae, "Rapid turning at high-speed: Inspirations from the cheetah's tail," in *2013 IEEE/RSJ International Conference on Intelligent Robots and Systems*, 2013: IEEE, pp. 5506-5511.

[18] A. Patel and M. Braae, "Rapid acceleration and braking: Inspirations from the cheetah's tail," in *2014 IEEE International Conference on Robotics and Automation (ICRA)*, 2014: IEEE, pp. 793-799.

[19] W. R. Provancher, S. I. Jensen-Segal, and M. A. Fehlberg, "ROCR: An Energy-Efficient Dynamic Wall-Climbing Robot," *IEEE/ASME Transactions on Mechatronics,* vol. 16, no. 5, pp. 897-906, 2011.

[20] W. Rone and P. Ben-Tzvi, "Dynamic Modeling and Simulation of a Yaw-Angle Quadruped Maneuvering With a Planar Robotic Tail," *J. Dyn. Syst. Meas. Control-Trans. ASME,* vol. 138, no. 8, p. 7, 2016.

[21] Y. J. Liu and P. Ben-Tzvi, "Dynamic modeling, analysis, and comparative study of a quadruped with bio-inspired robotic tails," *Multibody Syst. Dyn.,* vol. 51, no. 2, pp. 195-219, 2021.

[22] W. Saab, P. Ben-Tzvi, and Asme, "Design and Analysis of a Discrete Modular Serpentine Robotic Tail for Improved Performance of Mobile Robots," in *ASME International Design Engineering Technical Conference / Computer and Information in Engineering Conference (IDETC/CIE)*, Charlotte, NC, Aug 21-24 2016.

[23] W. Saab, W. S. Rone, and P. Ben-Tzvi, "Discrete modular serpentine robotic tail: design, analysis and experimentation," *Robotica,* vol. 36, no. 7, pp. 994-1018, 2018.
[24] W. Rone, W. Saab, P. Ben-Tzvi, and Asme, "Design, Modeling and Optimization of the Universal-Spatial Robotic Tail," in *ASME International Mechanical Engineering Congress and Exposition*, Tampa, FL, Nov 03-09 2017.
[25] W. S. Rone, Y. Liu, and P. Ben-Tzvi, "Maneuvering and stabilization control of a bipedal robot with a universal-spatial robotic tail," *Bioinspir. Biomim.,* vol. 14, no. 1, p. 16, 2019.
[26] W. S. Rone, W. Saab, and P. Ben-Tzvi, "Design, Modeling, and Integration of a Flexible Universal Spatial Robotic Tail," (in English), *J. Mech. Robot.,* vol. 10, no. 4, p. 14, 2018.
[27] Y. J. Liu, J. M. Wang, and P. Ben-Tzvi, "A Cable Length Invariant Robotic Tail Using a Circular Shape Universal Joint Mechanism," *J. Mech. Robot.,* vol. 11, no. 5, p. 14, 2019.
[28] W. Saab, S. Rone, A. Kumar, and P. Ben-Tzvi, "Design and Integration of a Novel Spatial Articulated Robotic Tail," (in English), *IEEE-ASME Trans. Mechatron.,* vol. 24, no. 2, pp. 434-446, 2019.
[29] W. S. Rone, W. Saab, A. Kumar, and P. Ben-Tzvi, "Controller Design, Analysis, and Experimental Validation of a Robotic Serpentine Tail to Maneuver and Stabilize a Quadrupedal Robot," *J. Dyn. Syst. Meas. Control-Trans. ASME,* vol. 141, no. 8, p. 9, 2019.
[30] Y. Liu and P. Ben-Tzvi, "Dynamic Modeling, Analysis, and Design Synthesis of a Reduced Complexity Quadruped with a Serpentine Robotic Tail," *Integrative and Comparative Biology,* vol. 61, no. 2, pp.464-477, 2021.
[31] B. G. Katz, "A low cost modular actuator for dynamic robots," Massachusetts Institute of Technology, 2018.
[32] Y. Liu and P. Ben-Tzvi, "Systematic Development of a Novel, Dynamic, Reduced Complexity Quadruped Robot Platform for Robotic Tail Research," *IEEE 2022 International Conference on Robotics and Automation*, May 23-27, 2022, Philadelphia, PA, USA.